Research Article Vol. 40, No. 4 / April 2023 / Journal of the Optical Society of America B 891

Journal of the Optical Society of America B

OPTICAL PHYSICS

Metalens integrated receiver to reduce the effect of angle of arrival jitter in free space optical communication

Md Shafiqul Islam,* Kaveh Shahverdi, and Ozdal Boyraz

Department of Electrical Engineering and Computer Science, University of California, Irvine, California 92697, USA
**msislam1@uci.edu*

Received 17 November 2022; revised 11 February 2023; accepted 23 February 2023; posted 27 February 2023; published 30 March 2023

In this paper, we propose a metalens integrated receiver for free space optical communication, which provides robust performance in the presence of angle of arrival fluctuations jitter. As a proof of concept, we show that our proposed receiver can tolerate up to a 2.5 mrad angle of arrival fluctuations with a detector radius of 20 μm before reaching a 3 dB power penalty. We design a meta unit cell to realize the optimized phase profile and present a quasi-3D full wave simulation of the proposed architecture. The system shows steady signal power and bit error rate in the presence of angle of arrival fluctuation.

https://doi.org/10.1364/JOSAB.481362

1. INTRODUCTION

Free space optical (FSO) communication has recently regained its momentum because of emerging applications, such as satellite-to-satellite communications, rapid rural area deployment, and data centers. It inherently provides high bandwidth, ease of deployment, license-free spectrum, low power consumption, and better channel security [1]. However, as a line of sight system, the FSO link requires precise alignment between transmitter and receiver. Misalignments lead to pointing errors and angle of arrival (AOA) fluctuations [2]; both cause performance degradation of the communication link. Pointing error is caused by transmitter vibration and turbulence in the propagating medium. The effect of pointing errors on the performance of the FSO system has been analyzed in numerous studies [3–5]. High-speed FSO links use broadband receivers with less than 50 μm detector diameter, and, hence, they can accept light from a limited field of view (FOV). As a result, fluctuation in the AOA severely affects FSO link performance [6]. To date, several active control systems have been proposed to mitigate fluctuations in the AOA and minimize the performance degradations [7,8]. Such active control systems require additional processing power and mechanical control that put stress on the size, weight, and power constraints of FSO communication. Adaptive beam size control by using an electrically focus-tunable lens is proposed in Ref. [2]. Although the system eliminates the mechanical components, the system still requires additional processing to dynamically reduce the AOA fluctuation. In all these systems due to slow response time and noise in the control systems, there is always a fast residual jitter in AOA, which significantly affects the bit error rate (BER) of the system [9].

In this paper, we propose a metalens integrated receiver system that provides robust performance in the presence of a jitter in the FSO link. The system performance degrades when the AOA deviates from the perfect alignment position, and, hence, the beam walks off on the detector plane. To maintain the BER like normal incidence, the system must pay a power penalty. For instance, a beam walk-off of 19.5 μm leads to a 3 dB power penalty in a typical conventional FSO system using an $f/10$ aperture lens followed by a detector with 20 μm radius. In other words, the system with 100 mm focal length tolerates up to 195 μrad AOA deviation with a 3 dB power penalty. Here, we show that the FSO receiver with a metalens maintains the same BER up to 2.5 mrad AOA deviation with less than 3 dB power penalty. The proposed metalens is based on a meta unit cell, which consists of amorphous silicon (a-Si) nanopillar on a quartz substrate. A full 2π phase shift with more than 93% transmission is achievable by varying the nanopillar diameter at the desired target wavelength. Here, we show how the metalens phase profile is optimized by using the receiver lens model available in commercial ray-tracing software and according to the location of the metalens in a conventional receiver system at a wavelength of 1 μm. Considering the efficiency and ease of fabrication, the proposed design can be tailored to other metasurfaces with optimized phase profiles. Since the system is static, free of mechanical parts, and requires no active control mechanisms, it provides a simple and easy-to-implement solution to reduce the effect of jitter on the FSO system performance. Also, further optimizations are possible for different aperture lenses to accommodate higher AOA variations.

The use of metasurfaces in electromagnetics and photonics was proposed five decades ago. In particular, metasurfaces have

emerged as a promising technology for wavefront shaping in optics due to their various useful properties, such as monolithic integration, compact design, and subwavelength control [10]. Metasurfaces have found applications in diffraction-limited focusing and imaging [11,12], polarization control [13], holography [14], and in an augmented reality/virtual reality system [15]. For imaging, a wide FOV metalens has been proposed in Refs. [16,17]. In these systems, a beam with different incident angles gets focused on different locations on the detector plane, and, hence, a detector array captures light for all incident angles. Mostly, such systems are designed for complementary metal-oxide semiconductor image sensors [18]. Since a single point detector is used in communication systems, the metalens design criteria differ from imaging systems that have been studied before. We previously presented a metalens receiver structure for the FSO that can capture wide range of incident angles [19]. However, the system works for a large f-number system. So, receiver systems with large apertures require long receivers, which are not feasible in some applications. Large aperture metalenses also pose fabrication challenges. In this paper, we modified a conventional receiver system with a bulk lens by incorporating a metalens. This paper provides design guidelines for such hybrid systems and potential improvements in system performance.

The paper is organized as follows. In Section 2, we describe our proposed receiver architecture. In Section 3, the impact of AOA variations in an ideal FSO receiver is analyzed. In Section 4, we present the results obtained by implementing our proposed architecture in an example system. In Section 5, we provide a meta unit cell design that can be used to realize a metalens with the desired phase profile. In Section 6, the effectiveness of the proposed system is shown by the full wave simulation. Finally, in Section 7, we discuss the maximum performance improvement from our system for different detector sizes.

2. PROPOSED SYSTEM

A simplified conventional receiver system is shown in Fig. 1(a). The system consists of an aperture lens with diameter a and focal length f, which focuses the light on a free space detector. A conventional system is designed in a way so that the detector captures the whole normally incident beam at the focal plane (AOA $= 0°$). In a real system, there is always some AOA fluctuation. AOA can deviate along both horizontal (x) and vertical (y) directions leading to horizontal (δ_x) and vertical (δ_y) beam walk-off on the detector plane. Let θ_x and θ_y be the deviations of the AOA along the x and y directions, respectively, then $\delta_x = f \tan(\theta_x)$ and $\delta_y = f \tan(\theta_y)$. The beam walk-off on the detector leads to degradation of the received power on the detector and, consequently, higher BER, which has been thoroughly investigated and modeled in the literature [20–22]. The level of degradation depends on the focused beam size, detector area, and focal length of the aperture lens. In all our following analyses, we will focus on nonzero δ_y only ($\delta_x = 0$). However, our system and analysis can easily be extended to the case where both δ's are nonzero. Because of the circular symmetry of the system, the performance will be similar.

The objective of the metalens is to correct the phase front of the beam so that the focal point remains the same for different AOA values. Since the phase front of the beam varies as the beam propagates in the receiver system, the metalens must be customized based on its specific location in the receiver. In our proposed system, the metalens is added to the focal plane of the aperture lens to alleviate the beam walk-off issue due to AOA fluctuation as shown in Fig. 1(b). The metalens redirects and focuses the incident beam with different AOAs to the center of the detector. To do that, the phase profile of the metalens should be $\phi(r) = br^2$. Here, r represents the radial coordinate of the points on the plane of the metalens. Parameter b is the phase constant that needs to be optimized such that the beam with $\theta_y = \theta_{\text{opt}}$ will be focused on the center of the detector. We chose

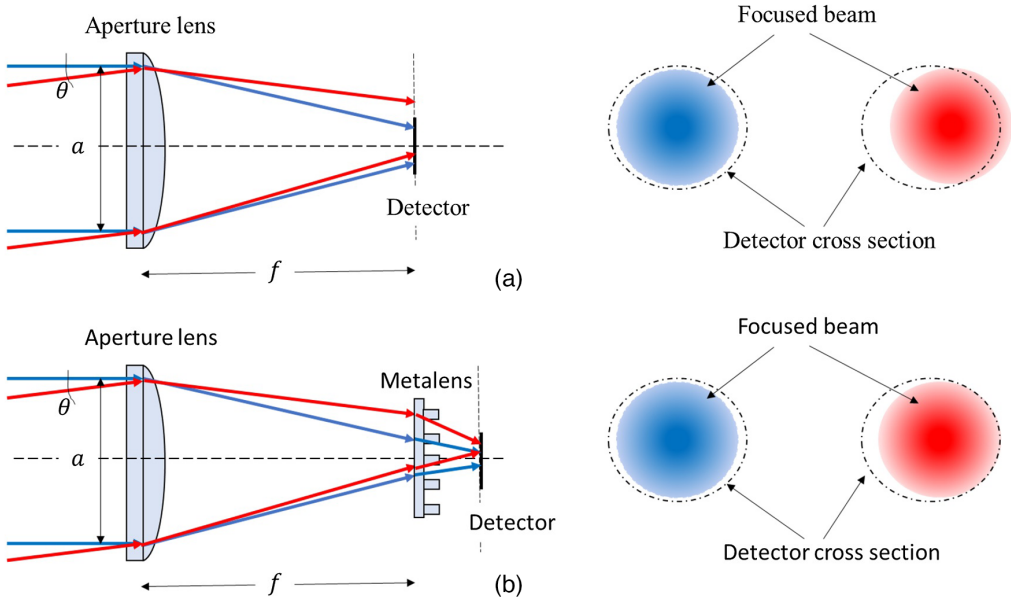

Fig. 1. (a) Conventional receiver with normal and oblique incident beams (left). Beam walk-off on the detector plane in the conventional receiver for normal (blue) and oblique (red) incident beams (right). (b) Proposed receiver with normal and oblique incident beams (left). Beam walk-off on the detector plane in the proposed receiver for normal (blue) and oblique (red) incident beams (right).

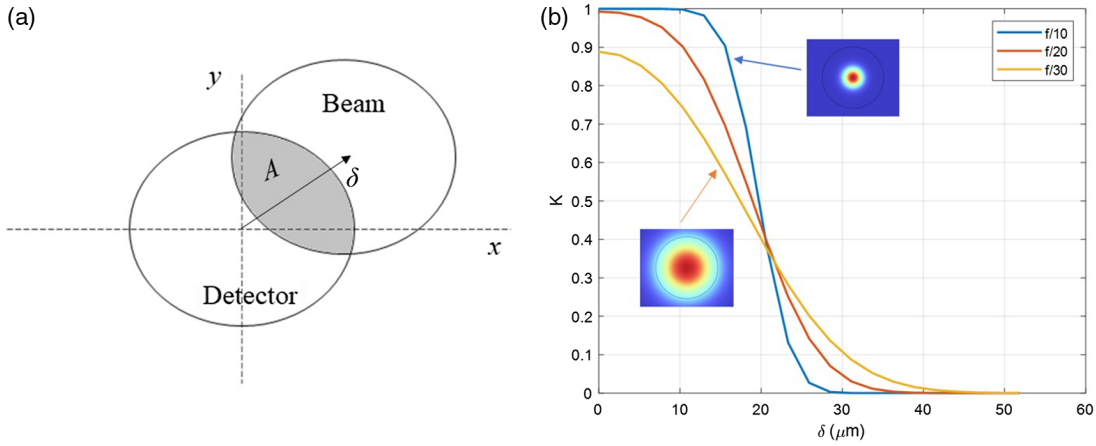

Fig. 2. (a) Detector and beam overlap area (gray shaded region) for calculation of power degradation factor K. (b) K versus beam walk-off (δ) for an ideal system with a detector radius of 20 μm. The insets show the beam profile in arbitrary units (a.u.) for $f/10$ and $f/30$ systems where the solid black circle represents the detector boundary.

θ_{opt} to be the maximum expected AOA of the communication link $\theta_{\text{opt}} = \theta_m$. In this way, beam walk-off for all the angles $-\theta_m < \theta_y < \theta_m$ will be improved compared to the conventional receiver system. The coefficient b can also be obtained analytically by applying the generalized Snell law [23].

Our chosen phase profile is quadratic, which can lead to spherical aberration for a large metalens. However, as we place the metalens near the focus of the aperture lens, the required metalens diameter is small (less than $100 \sim$ μm). So, we expect that the effect of spherical aberration from the metalens will be negligible. However, aberration from the aperture lens needs to be considered as it can change the shape of the focused beam after the metalens.

3. EFFECT OF ANGLE OF ARRIVAL VARIATION

The beam walk-off can reduce the power captured by the detector. The reduction can be quantified by the performance degradation factor K. We define $K = P_d/P_{\text{av}}$, where P_d is the power received by the (finite-sized) detector, and P_{av} is the total power available at the (infinite) detector plane. If the focusing optics is lossless, we get $P_{\text{av}} = P_{\text{rec}}$ where P_{rec} is the total optical power received by the receiver aperture. The performance degradation factor K can be obtained from the focused beam intensity distribution on detector plane $I_d(x, y)$ as shown below:

$$K = \frac{\iint_A I_d(x - \delta_x, y - \delta_y)\mathrm{d}x\mathrm{d}y}{\iint I_d(x, y)\mathrm{d}x\mathrm{d}y}. \quad \textbf{(1)}$$

Here, the integration in the numerator is carried out only on detector area A, which is illuminated by the focused beam [as shown in Fig. 2(a)], and the integration in the denominator is carried over the full beam area. With no beam walk-off ($\delta_x = \delta_y = 0$), K attains its maximum value of K_0. K_0 depends on detector size and $K_0 = 1$, when the detector is large enough to capture the full beam. Due to rotational symmetry, K is only function of radial beam walk-off $\delta = \sqrt{\delta_x^2 + \delta_y^2}$. In an ideal system, we assume that the Gaussian beam with beam diameter $2w_0$ is incident on a lossless aberration-free aperture lens with focal length f. The focused beam is then also Gaussian with the beam diameter, $2w = \frac{4\lambda f}{\pi(2w_0)} = \frac{4\lambda}{\pi} \times f-\text{number}$ [24]. Here, λ is the wavelength of light. We chose $I_d(x, y) = \frac{2}{\pi w^2}\exp[-2(x^2 + y^2)/w^2]$ so that the integration in the denominator of Eq. (1) always remains 1, and we only need to run numerical integration over the finite area of A. The variation of K with radial beam walk-off (δ) for a different f number of the aperture lens is shown in Fig. 2(b) with detector radius (r_d) of 20 μm. Note that for an $f/30$ aperture lens, the beam size is larger than the detector area and, hence, K is less than 1 even for normal incidence.

The incident optical signal on the detector generates photocurrent that depends on detector responsivity, R and optical power on the detector, and $P_d = P_{\text{rec}}K$ (assuming $P_{\text{rec}} = P_{\text{av}}$). The photocurrent also contains a noise component n, which arises due to several factors, such as shot noise, dark current, thermal noise, avalanche photodetector excess noise factor, flicker noise, etc. The overall photocurrent can be modeled as $i_d = P_{\text{rec}}KR + n$. Here, for proof of concept, we focus on on–off keying (OOK) modulation where the received signal can have two power levels 0 and P_{rec} for bits 0 and 1, respectively. The BER can be calculated using the following formula:

$$\text{BER}(K) = \frac{1}{2}\left[Q\left(\frac{P_{\text{Th}}}{\sigma_n}\right) + Q\left(\frac{P_{\text{rec}}K - P_{\text{Th}}}{\sigma_n}\right)\right]. \quad \textbf{(2)}$$

Here, $Q(\ldots)$ represents the Q function, and σ_n is the variance of the detector noise n. Although only OOK is presented here, the results can be extended to coherent communication systems or systems using block codes. Since all modulation formats benefit from increased power efficiency, we anticipate that reducing the jitter will improve the BER and maximum reach of alternative modulation schemes.

In our calculation, we assume the responsivity of the photodiode is $R = 1$. [For the detector with different responsivities, both systems will suffer from same power penalty. However, still our system will show less power fluctuation from the angle of

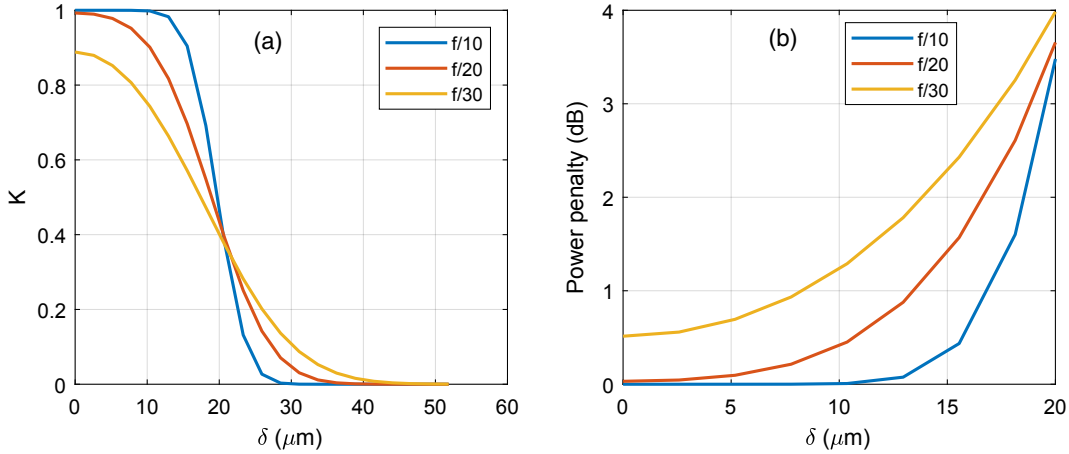

Fig. 3. (a) BER and (b) power penalty for an ideal conventional system with a detector radius of 20 μm.

arrival variation due to reduced beam walk-off.] The decision level threshold is assumed fixed as $P_{\mathrm{Th}} = \frac{P_{\mathrm{rec}}}{2}$, where P_{rec} is the received power for normally incident beam on aperture lens in the receiver system. The fixed P_{Th} approximation is justified as it is not possible to dynamically adjust P_{Th} with the fast variation of AOA. The BER variation with K is shown in Fig. 3(a). We assume that in system design P_{rec} is selected so that BER $\approx 10^{-12}$ at AOA $= 0$ assuming full beam power is available on the detector $P_d = P_{\mathrm{rec}}$. Here, we present our result considering the angle of arrival has a uniform variation. However, in a realistic system, the beam wandering, and phase front distortions will cause stochastic variations in the received power and angle of arrival. Neglecting the effect of turbulence, we can calculate the statistical average of the BER as $E[\mathrm{BER}] = \int_0^\infty p(\delta)\,\mathrm{BER}(\delta)\,\mathrm{d}\delta$. Here, $p(\delta)$ is the probability density function of the radial beam walk-off. The beam walk-off along two orthogonal directions is assumed to be independent random variables with the Gaussian distribution of variance σ and mean zero. Then, $p(\delta)$ turns out to be Rayleigh distribution $p(\delta) = \frac{\delta}{\sigma^2}\exp - (\delta^2/2\sigma^2)$ [5]. By using a suitable PDF, we can also include the effect of turbulence in the proposed system.

When the performance degradation factor is less than 1, excess power is needed to maintain the same BER as $K = 1$. Such a power penalty can be calculated from K as power penalty $(\mathrm{dB}) = 10\log_{10}(K)$. The power penalty for a conventional system with respect to the variation of the beam walk-off is also shown in Fig. 3(b).

4. RESULTS

As a proof of concept, here, we designed and analyzed a system consisting of an aperture lens with an aperture diameter of $a = 10$ mm and a focal length of $f = 100$ mm ($f/10$ system). We used a commercially available lens model in OpticStudio to perform ray-based and physical optics-based simulations. (The simulation model also incorporates the effects of aberration from the aperture lens). The operating wavelength is 1 μm. Initially, we design the system for $\theta_{\mathrm{opt}} = 1$ mrad. From ray-based simulation, optimized phase constant b is found to be $-6188.907\ \mathrm{rad/mm^2}$. The "binary 2" surface feature in OpticStudio is used to simulate the metalens. The ray diagrams for the conventional receiver and our proposed receiver are shown in Figs. 4(a) and 4(b), respectively. We calculated the beam walk-off for the AOA ranging from 0 to 1 mrad. It is observed that our designed system can significantly reduce the beam walk-off for the large range of the AOA [Fig. 4(c)]. Due to reduced beam walk-off, the captured optical power for the fixed radius optical detector is improved. Physical optics propagation (POP) simulation is carried out to calculate the power degradation factor, and the associated power penalty with the AOA for a detector with radius 20 μm. The results are shown in Figs. 5(a) and 5(b), respectively. For POP simulation, a Gaussian beam with beam waist $w_0 = 5$ mm (beam diameter $2w_0 = 10$ mm) is used as the input beam. For the non-Gaussian beam shape, we expect a slight variation in beam width due to the diffraction effect. However, the beam walk-off will remain the same. Using K for each AOA, we calculated the BER for both conventional and proposed systems. As shown in Fig. 5(c), the BER for the conventional system degrades for the larger AOA, but it remains almost same for our proposed system. Here, the BER for our system is worse than the conventional system at normal incidence for the same P_{rec} as the beam expands before reaching the detector [Fig. 4(b)]. Bigger spot size on the focus of the aperture lens will help reducing the spot size on detector and will, thus, improve the BER. By simple calculation, we can show that when our system's f number is greater than 19.8, the detector with radius 20 μm can capture the full beam, leading to $K = 1$ for normal incidence and, thus, minimum BER. The average BER, $E[\mathrm{BER}]$ for different jitter variance σ is presented in Fig. 5(d). Relatively constant BER with the AOA leads to almost fixed $E[\mathrm{BER}]$ for our proposed system, whereas, for the conventional system, $E[\mathrm{BER}]$ significantly degrades for a variance greater than 25 μrad. Conventional and proposed systems both perform better with larger detector area. Thus, our proposed system shows robust performance in the presence of AOA fluctuation. In our design, the phase constant b is optimized for a fixed location along optical axis with the metalens surface perfectly normal to the optical axis. After b is optimized, an offset in the metalens position along optical axis z can change beam walk-off and, hence, can change K. Due to angular invariance in the phase profile, tilt around the optical axis cannot alter K, but tilt along other axes will degrade K. In the next section, we present a

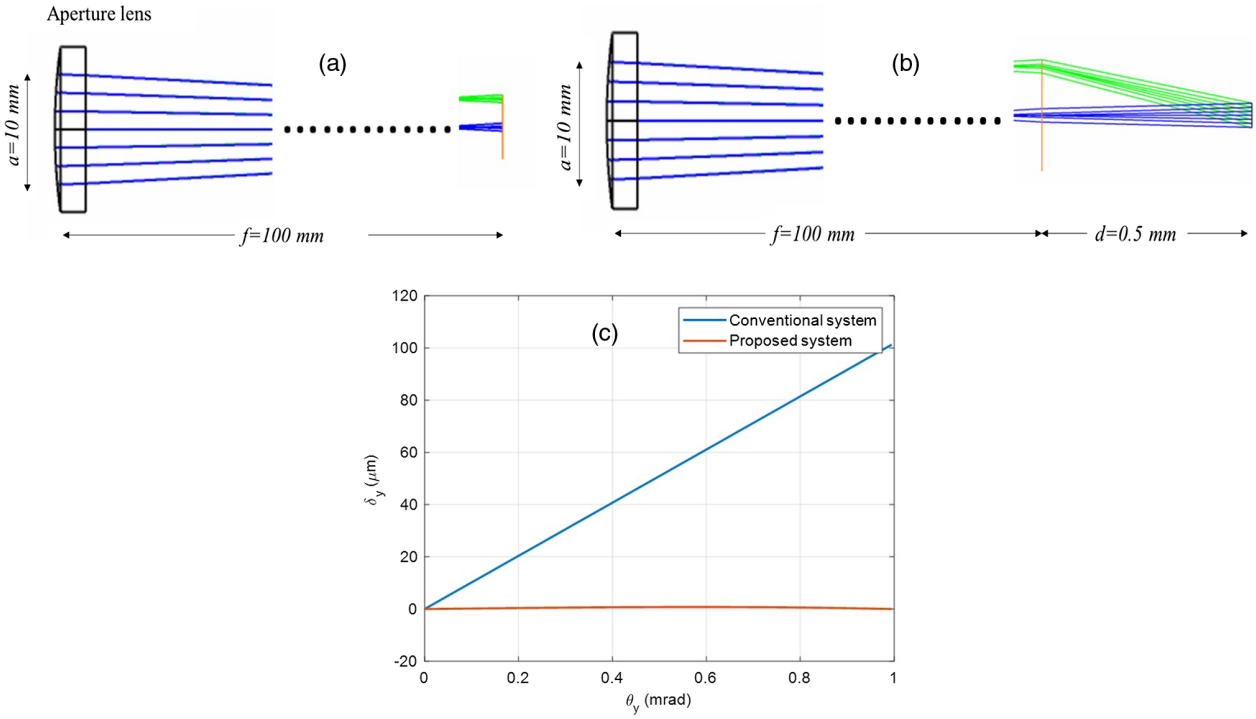

Fig. 4. (a) Ray diagram for the conventional receiver. (b) Ray diagram for the proposed receiver. Blue rays indicate AOA = 0 rad, and the green rays indicate AOA = 1 mrad. (c) Beam walk-off (δ_y) for different AOA (θ_y)'s.

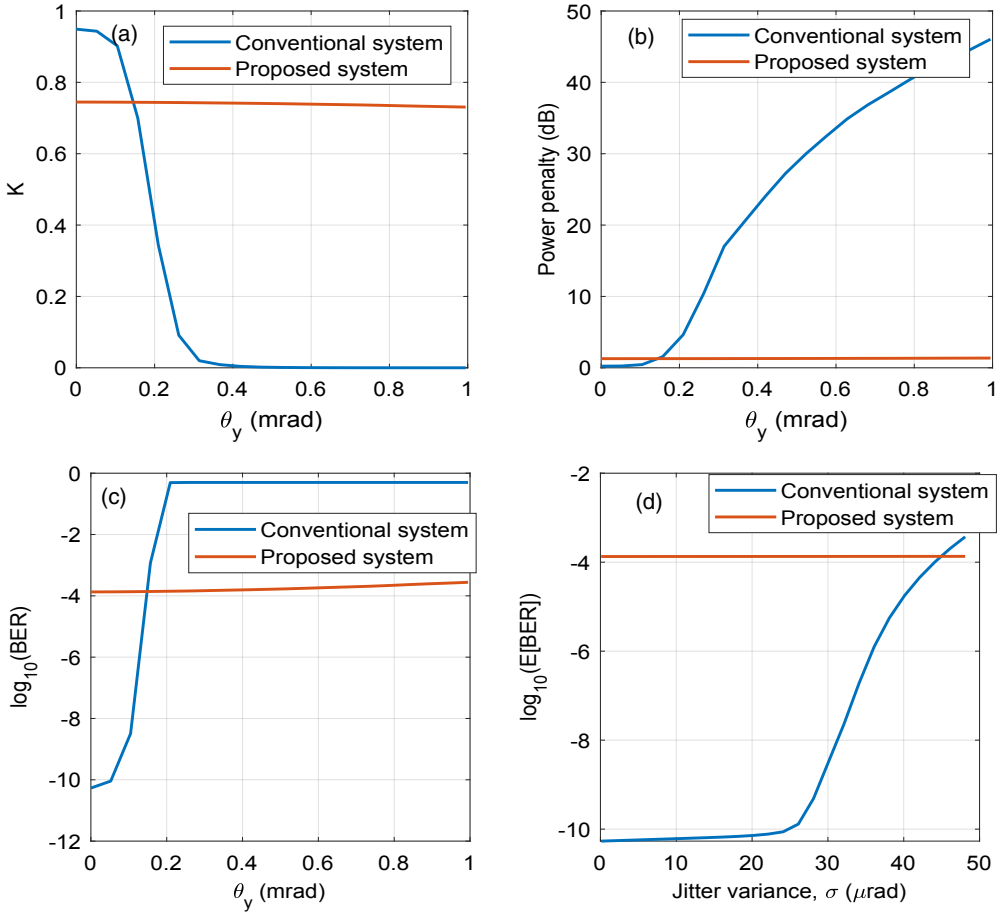

Fig. 5. (a) Power degradation factor (K), (b) power penalty, and (c) BER variation with AOA (θ_y) for the conventional and proposed receivers with the detector radii of 20 μm. E[BER] for different jitter variances is shown in (d).

meta unit-cell structure that can be used to realize the optimized phase profile we obtained in this section.

5. META UNIT CELL

We propose a meta unit cell consisting of an a-Si nanopillar on a 200 nm thick quartz substrate. We optimized the physical dimension of the unit cell [separation between the unit cell (U) and height (H) of the nanopillar] so that we can obtain a full 2π phase shift with high transmission by varying nanopillar diameter D. The optimized values are $H = 450$ nm and $U = 350$ nm. Full wave simulations based on the finite element method (FEM) are carried out in COMSOL MULTIPHYSICS for a unit cell with the periodic boundary condition in transverse boundaries. The refractive indices of 3.80 and 1.45 are assumed for a-Si and quartz, respectively [25]. The plane wave is normally incident from the quartz side and transmission S-parameter S21 is calculated. Multiple simulations are performed for various nanopillar diameters. The relative transmission phase for different nanopillar diameters is calculated considering the phase at 310 nm diameter as a reference. Using this platform, we obtained transmission greater than 93% and a full 2π phase shift by varying the nanopillar diameter from 100 to 310 nm (Fig. 6). Due to circular symmetry, the proposed unit cell is polarization insensitive. Such a metalens can be fabricated by using electron-beam lithography [26] or by direct pattering on a quartz substrate by using deep ultraviolet photolithography [27,28].

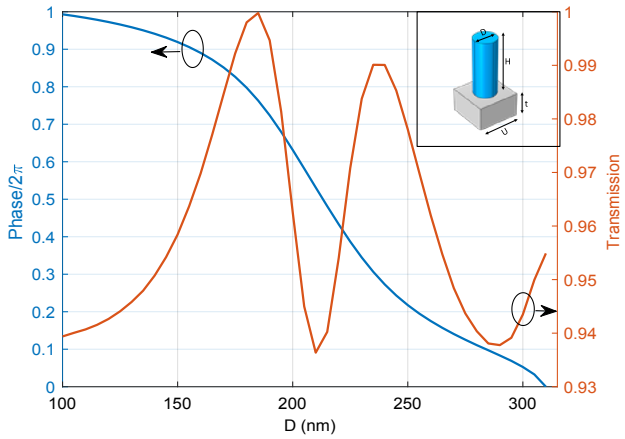

Fig. 6. Transmission magnitude and phase variations of the normally incident beam on meta-unit-cell structure with respect to the diameter D of the unit cell. The meta unit cell is shown in the inset.

6. FULL WAVE SIMULATION OF THE METALENS INTEGRATED RECEIVER

Full wave simulation of the full receiver system requires high computational resources. To make the simulation manageable, we divide our system in several subsystems as shown in Fig. 7(a), and only the region near the metalens is simulated by the full wave simulation (FEM). First, the POP based on the diffraction theory is carried out in OpticStudio to find the beam profile at the focal plane of the aperture lens. The physical optics method provides a fast and low complexity estimation of the scattered field with a good level of accuracy if the wavelength of the incident wave is significantly smaller than the radius of the curvature of the lens. Only E_x polarization is considered for simulation simplification. From the 2D beam profile, the beam along the $x = 0$ cross section is selected as the input reference for

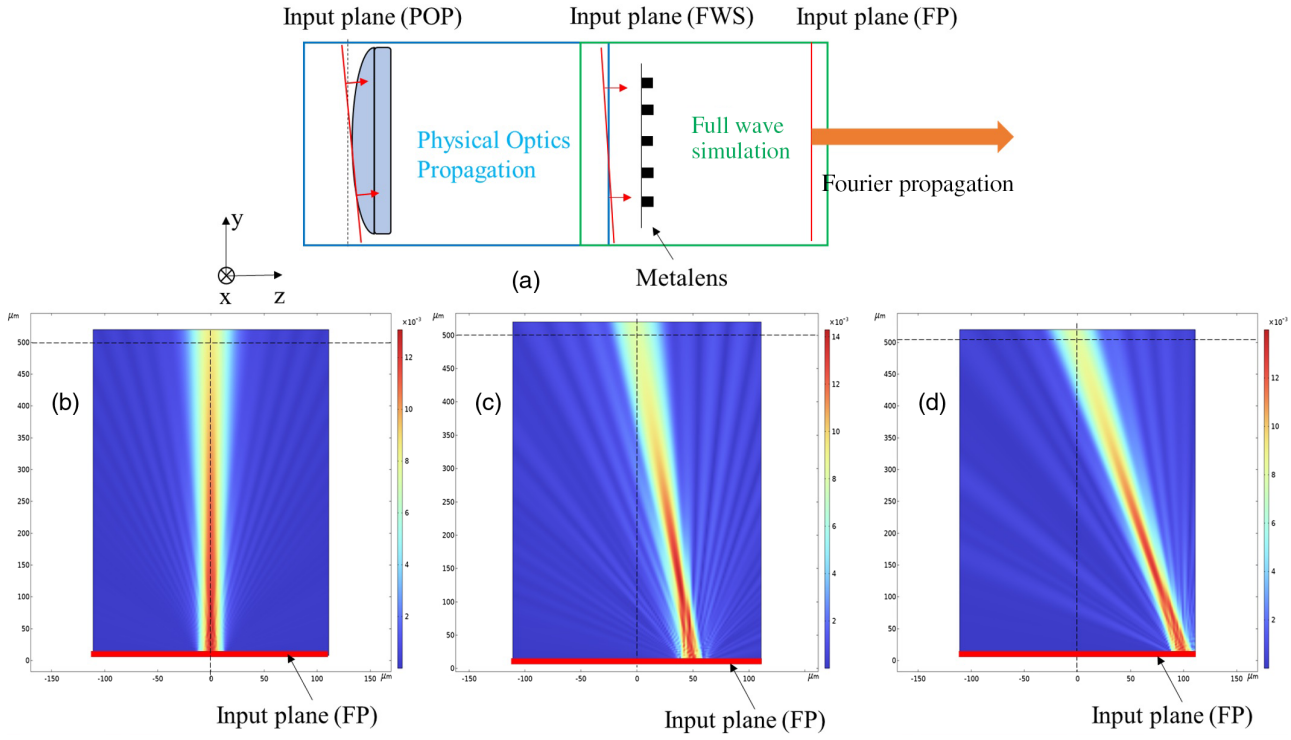

Fig. 7. (a) Simulation block diagram. Fourier propagation result for (a) $\theta_y = 0$ mrad, (b) and (c) $\theta_y = 0.5$ mrad, and (d) $\theta_y = 1$ mrad. Field values are in a.u.

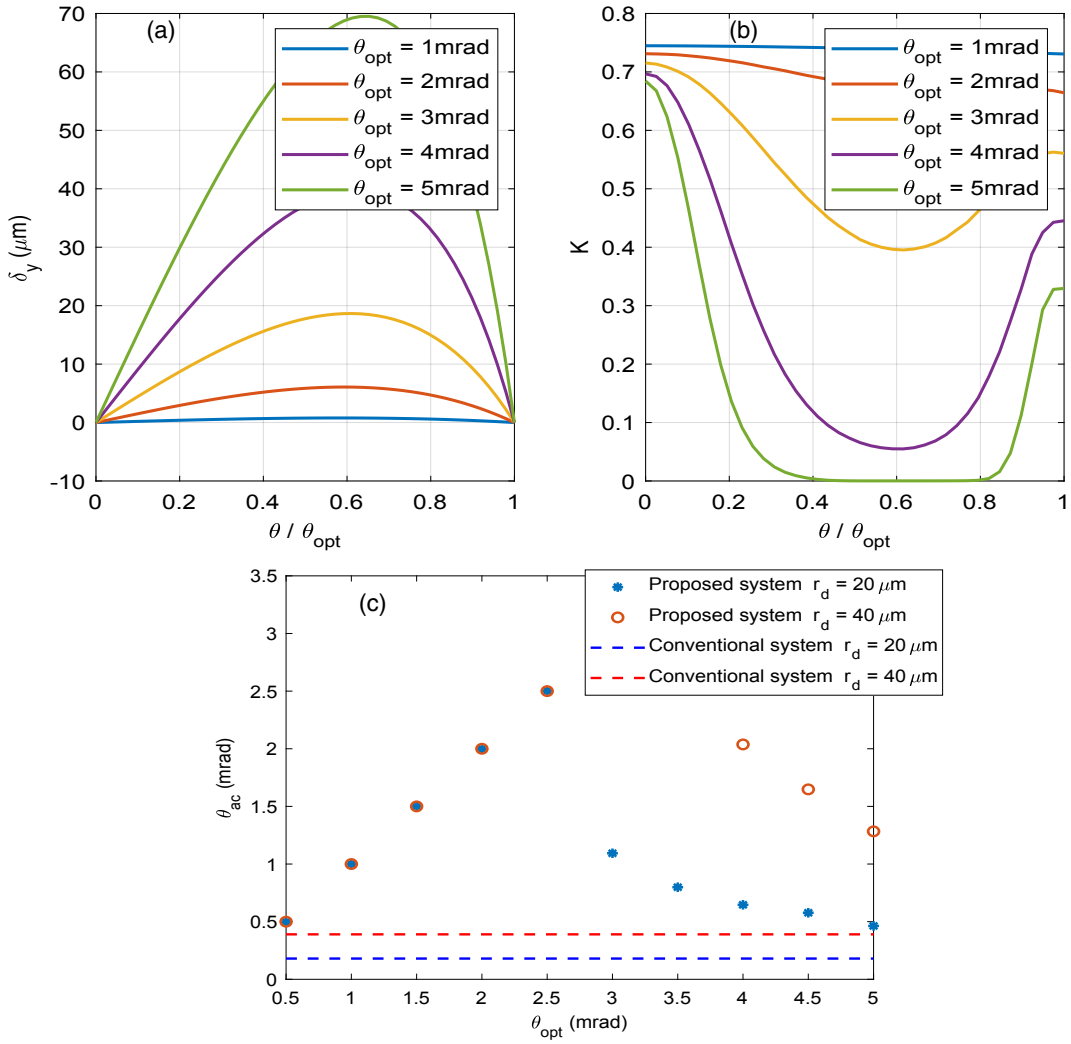

Fig. 8. (a) Beam walk-off δ_y, (b) perform degradation factor, K, with different θ/θ_{opt}'s. (c) Region of operation for different θ_{opt}'s based on $K_{tol} = 0.5$ criteria.

the full wave simulation. It is assumed that the beam is uniform along the x direction (quasi-2D beam profile). In quasi-3D simulation, we design only a single row of the metalens based on the $x = 0$ cross-sectional phase pattern $[\phi(y) = by^2]$. Along the x direction, we used the periodic boundary condition so the input beam and metalens rows are both invariant along the x direction. The width along the x direction is set as a period of metalens U. As $U < \lambda$, only 0th order (normal) propagation exists along the x direction. The desired phase $\phi(y)$ of the metalens is sampled with separation U and nanopillars with diameter giving the sampled phase are placed on appropriate location. The input field profile is excited by defining magnetic surface current densities ($\vec{M}_s = \vec{n} \times \vec{E}$). Perfectly matched layer is applied in all the other boundaries to eliminate unwanted backscattering to the simulation domain. The beam profile on a plane in front of a metalens is captured and used as the input field for final Fourier optics-based calculation. Beam evolution after the metalens for three different incident angles (0, 0.5, and 1 mrad) are shown in Figs. 7(b)–7(d). In all cases, the beams go through the detector sitting 500 μm away from the metalens plane. We estimate K as 0.82, 0.79, and 0.80 for 0 mrad, 0.5 mrad, and 1 mrad, respectively. Physical Optics simulation gives a K value around 0.74. The discrepancy arises for several reasons. The POP simulation assumes the metalens is 100% efficient. Quasi-3D full wave simulation includes metalens-scattering losses for 1D aperiodic arrangement of varying nanopillar diameter. In the real lens, nanopillar diameter would be varied along the 2D plane, and the efficiency will be lower than the one obtained in quasi-3D simulation. With 80% efficiency for the 1D phase variation, we estimate efficiency of 64% for the 2D phase profile variation. Although, a conventional lens can be more efficient (>95%), we cannot achieve similar functionality of the metalens. This degradation in power by the metalens can be compensated by increasing the system's power budget. Here, we realized the desired quadratic phase profile by placing the nanopillar with a corresponding diameter in the appropriate location. Due to fabrication inaccuracy, the nanopillar diameter may vary. This will change the phase imparted by the metalens. By using the uniform diameter inaccuracy distribution, we find out that the rms phase variation

can be as much as 0.05 rad and 0.01 rad for max diameter deviations of 1 nm and 5 nm, respectively. A further study should be conducted based on real fabrication inaccuracies to evaluate potential scattering losses and beam smearing.

7. REGION OF OPERATION

In our proposed system, phase coefficient b is calculated so that the beam walk-off for $\theta_y = \theta_{\text{opt}}$ will be zero. For other $\theta_y < \theta_{\text{opt}}$, the beam walk-off ($\delta_y$) is not exactly zero. If the beam walk-off is significantly large, the system will not have acceptable performance. To have an idea about how large the AOA can be, we designed the system for θ_{opt} up to 5 mrad. We calculated the beam walk-off for $\theta < \theta_{\text{opt}}$ in each design. The result is presented in Fig. 8(a). The beam walk-off can be significantly high especially when the system is designed for larger θ_{opt}. Large beam walk-off will result in a lower K value and a wide variation of K for different $\theta < \theta_{\text{opt}}$'s [Fig. 8(b)]. This behavior sets a limit on the maximum allowable AOA in our proposed system. The maximum allowable AOA can be defined based on the tolerance level of K for a specific system. We can define the active region of operation θ_{ac} for our proposed system based on the tolerance level of K (K_{tol}) such that

$$\theta_{\text{ac}} = \begin{cases} \theta_{\text{opt}}, & \text{when } \theta_k > \theta_{\text{opt}} \\ \theta_k, & \text{when } \theta_k < \theta_{\text{opt}} \end{cases}. \tag{3}$$

Here, θ_k is the minimum angle at which $K = K_{\text{tol}}$. When δ_x and δ_y both are nonzero, our system works for all possible angles (θ_x, θ_y) inside a circle with radius θ_{ac} on the $\theta_x - \theta_y$ plane. If we select $K_{\text{tol}} = 0.5$, θ_{ac} for different θ_{opt}'s is shown in Fig. 8(c). For comparison, θ_{ac} for the conventional system (angle at which $K = 0.5$) is also shown. This analysis shows that we cannot increase θ_{ac} by optimizing b for larger θ_{opt}. However, still our proposed system offers significant improvement over the conventional system. For a 20 μm detector radius, our proposed system can tolerate the AOA of up to 2.5 mrad, whereas, the conventional system can only tolerate less than 200 μrad. For a larger detector radius, our proposed receiver can even tolerate larger AOA variations.

8. CONCLUSION

In this paper, we proposed the use of the metalens in optical receiver design for free space optical communication. Our proposed receiver with an integrated metalens showed robust performance in the presence of the AOA jitter. We obtained significant performance improvement (power penalty and BER) compared to the conventional receiver by incorporating the metalens in the receiver system. Metalens/metasurface allowed arbitrary wavefront control, which can be utilized in situations where the bulk conventional lens was not applicable. We believe that such wide functionality of the metalens is highly desirable and useful to solve many different problems in the FSO system.

Disclosures. The authors declare no conflicts of interest.

Data availability. Data underlying the results presented in this paper are available upon request.

REFERENCES

1. H. Kaushal and G. Kaddoum, "Optical communication in space: challenges and mitigation techniques," IEEE Commun. Surv. Tuts. **19**, 57–96 (2017).
2. V. V. Mai and H. Kim, "Beam size optimization and adaptation for high-altitude airborne free-space optical communication systems," IEEE Photon. J. **11**, 7902213 (2019).
3. C.-C. Chen and C. S. Gardner, "Impact of random pointing and tracking errors on the design of coherent and incoherent optical intersatellite communication links," IEEE Trans. Commun. **37**, 252–260 (1989).
4. D. K. Borah and D. G. Voelz, "Pointing error effects on free-space optical communication links in the presence of atmospheric turbulence," J. Lightwave Technol. **27**, 3965–3973 (2009).
5. A. A. Farid and S. Hranilovic, "Outage capacity optimization for free-space optical links with pointing errors," J. Lightwave Technol. **25**, 1702–1710 (2007).
6. S. Huang and M. Safari, "Free-space optical communication impaired by angular fluctuations," IEEE Trans. Wireless Commun. **16**, 7475–7487 (2017).
7. E. Ciaramella, Y. Arimoto, G. Contestabile, M. Presi, A. D'Errico, V. Guarino, and M. Matsumoto, "1.28 terabit/s (32 × 40 Gbit/s) WDM transmission system for free space optical communications," IEEE J. Sel. Areas Commun. **27**, 1639–1645 (2009).
8. A. M. Brown, D. V. Hahn, D. M. Brown, N. W. Rolander, C.-H. Bair, and J. E. Sluz, "Experimental implementation of fiber optic bundle array wide FOV free space optical communications receiver," Appl. Opt. **51**, 3995–4002 (2012).
9. I. U. Zaman and O. Boyraz, "Impact of receiver architecture on small satellite optical link in the presence of pointing jitter," Appl. Opt. **59**, 10177–10184 (2020).
10. A. H. Dorrah and F. Capasso, "Tunable structured light with flat optics," Science **376**, eabi6860 (2022).
11. M. Khorasaninejad, W. T. Chen, R. C. Devlin, J. Oh, A. Y. Zhu, and F. Capasso, "Metalenses at visible wavelengths: diffraction-limited focusing and subwavelength resolution imaging," Science **352**, 1190–1194 (2016).
12. M. Veysi, C. Guclu, O. Boyraz, and F. Capolino, "Thin anisotropic metasurfaces for simultaneous light focusing and polarization manipulation," J. Opt. Soc. Am. B **32**, 318–323 (2015).
13. Y. Hu, X. Wang, X. Luo, X. Ou, L. Li, Y. Chen, P. Yang, S. Wang, and H. Duan, "All-dielectric metasurfaces for polarization manipulation: principles and emerging applications," Nanophotonics **9**, 3755–3780 (2020).
14. R. Zhao, L. Huang, and Y. Wang, "Recent advances in multi-dimensional metasurfaces holographic technologies," PhotoniX **1**, 20 (2020).
15. G.-Y. Lee, J.-Y. Hong, S. Hwang, S. Moon, H. Kang, S. Jeon, H. Kim, J.-H. Jeong, and B. Lee, "Metasurface eyepiece for augmented reality," Nat. Commun. **9**, 4562 (2018).
16. B. Groever, W. T. Chen, and F. Capasso, "Meta-lens doublet in the visible region," Nano Lett. **17**, 4902–4907 (2017).
17. M. Y. Shalaginov, S. An, F. Yang, P. Su, A. Agarwal, H. Zhang, J. Hu, and T. Gu, "Single-layer planar metasurface lens with >170° field of view," in *Frontiers in Optics + Laser Science APS/DLS* (OSA, 2019), paper FM4C.1.
18. J. Ma, D. S. Robledo, L. Anzagira, D. Zhang, K. Shahverdi, and S. Masoodian, "A 1.26-inch 40.7 mega-pixel photon-counting quanta image sensor with 0.35e- read noise and 95 dB single-exposure dynamic range," in *Imaging and Applied Optics Congress 2022 (3D, AOA, COSI, ISA, PcAOP)* (Optica Publishing Group, 2022), paper JW5B.4.
19. M. S. Islam, I.-U. Zaman, P. Sadri-Moshkenani, M. W. Khan, and O. Boyraz, "Metalens wide-angle receiver for free space optical communications," Proc. SPIE **11814**, 48–53 (2021).
20. C. Zhai, L. Tan, S. Yu, and J. Ma, "Fiber coupling efficiency for a Gaussian-beam wave propagating through non-Kolmogorov turbulence," Opt. Express **23**, 15242–15255 (2015).
21. J. Sun, P. Huang, and Z. Yao, "Fiber-coupling efficiency for satellite-to-ground laser links with angle-of-arrival fluctuations," in *IEEE 19th International Conference on Communication Technology (ICCT)* (2019), pp. 705–709.

22. X. Ke and Z. Tan, "Effect of angle-of-arrival fluctuation on heterodyne detection in slant atmospheric turbulence," Appl. Opt. **57**, 1083–1090 (2018).
23. N. Yu, P. Genevet, M. A. Kats, F. Aieta, J.-P. Tetienne, F. Capasso, and Z. Gaburro, "Light propagation with phase discontinuities: generalized laws of reflection and refraction," Science **334**, 333–337 (2011).
24. S. A. Self, "Focusing of spherical Gaussian beams," Appl. Opt. **22**, 658–661 (1983).
25. T. Hu, Q. Zhong, N. Li, Y. Dong, Y. H. Fu, Z. Xu, D. Li, V. Bliznetsov, K. H. Lai, S. Zhu, Q. Lin, Y. Gu, N. Singh, and D.-L. Kwong, "Demonstration of a-Si metalenses on a 12-inch glass wafer by CMOS-compatible technology," arXiv, arXiv:1906.11764v1 (2019).
26. Y. F. Yu, A. Y. Zhu, R. Paniagua-Domínguez, Y. H. Fu, B. Luk'yanchuk, and A. I. Kuznetsov, "High-transmission dielectric metasurface with 2π phase control at visible wavelengths," Laser Photon. Rev. **9**, 412–418 (2015).
27. Q. Zhong, Y. Dong, D. Li, N. Li, T. Hu, Z. Xu, Y. Zhou, K. H. Lai, Y. H. Fu, V. Bliznetsov, H.-J. Lee, W. L. Loh, S. Zhu, Q. Lin, and N. Singh, "Large-area metalens directly patterned on a 12-inch glass wafer using immersion lithography for mass production," in *Optical Fiber Communication Conference (OFC)* (OSA, 2020), pp. 1–3.
28. L. Zhang, S. Chang, X. Chen, Y. Ding, M. T. Rahman, Y. Duan, M. Stephen, and X. Ni, "High-efficiency, 80 mm aperture metalens telescope," Nano Lett. **23**, 51–57 (2023).